Langmuir

Article

pubs.acs.org/Langmuir

Bubble-Propelled Micromotors for Enhanced Transport of Passive Tracers

Jahir Orozco,[†] Beatriz Jurado-Sánchez,[†] Gregory Wagner,[‡] Wei Gao,[†] Rafael Vazquez-Duhalt,[†] Sirilak Sattayasamitsathit,[†] Michael Galarnyk,[†] Allan Cortés,[†] David Saintillan,*[,‡] and Joseph Wang*[,†]

[†]Department of Nanoengineering, University of California San Diego, La Jolla, California 92093, United States

[‡]Department of Mechanical and Aerospace Engineering, University of California San Diego, La Jolla, California 92093, United States

Supporting Information

ABSTRACT: Fluid convection and mixing induced by bubble-propelled tubular microengines are characterized using passive microsphere tracers. Enhanced transport of the passive tracers by bubble-propelled micromotors, indicated by their mean squared displacement (MSD), is dramatically larger than that observed in the presence of catalytic nanowires and Janus particle motors. Bubble generation is shown to play a dominant role in the effective fluid transport observed in the presence of tubular microengines. These findings further support the potential of using bubble-propelled microengines for mixing reagents and accelerating reaction rates. The study offers useful insights toward understanding the role of the motion of multiple micromotors, bubble generation, and additional factors (e.g., motor density and fuel concentration) upon the observed motor-induced fluid transport.

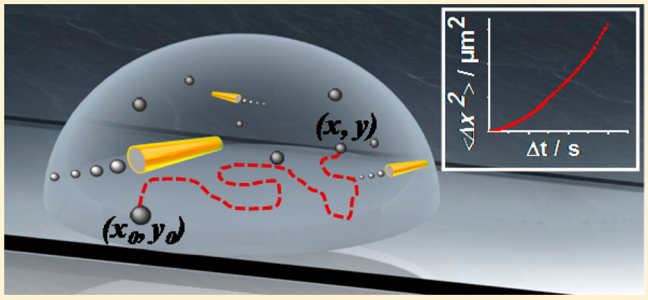

INTRODUCTION

Micromotors, unlike their macroscale counterparts, operate in the low Reynolds number regime where inertial forces are dominated by viscous stresses, and are thus subject to significant constraints on the method of propulsion and analysis of their motions.[1−9] Particular recent attention has been given to chemically powered micromotors, including bimetallic nanowires,[10,11] tubular microengines,[12−15] and Janus microparticles,[16−19] that exhibit autonomous self-propulsion in the presence of hydrogen peroxide fuel. Tubular microengines have attracted substantial interest due to their remarkable cargo-towing[20,21] and solution-mixing capabilities in different environments toward diverse biomedical[22−25] and environmental[26−28] applications. For example, the continuous movement of tubular microengines has been shown to be extremely effective in accelerating detoxification and decontamination reactions.[27,28] The dramatically accelerated remediation of chemical pollutants and threats has been attributed to an efficient motor-induced fluid mixing (without external agitation). Such fluid mixing capability of these tubular microengines holds a considerable promise for enhancing the yield and speed of a wide range of chemical processes, where quiescent conditions lead to low reaction efficiencies and long reaction times.

Herein, we present a fundamental study of the dramatically enhanced fluid transport observed in the presence of bubble-propelled tubular microengines using passive microparticle tracers. The displacement of passive microparticle tracers has been previously used for studying enhanced diffusion processes associated with the motility of *E. coli* bacteria,[29−31] and more recently with the movement of catalytic nanowire and Janus motors.[32,33] The substantial fluid transport associated with the movement of catalytic tubular microengines is characterized in the next sections by analyzing the mean squared displacement (MSD) of passive polystyrene bead tracers over different time scales. Our new findings provide strong evidence that the long tail of oxygen microbubbles generated in the catalytic cavity of the tubular microengines plays a crucial role in the dramatically enhanced displacement of passive bead tracers. Our data also demonstrates that the tracer displacement is substantially larger than that observed in the presence of other catalytic micromotors, including bimetal nanowires and Pt-based Janus particles. The new knowledge of the microengine-induced fluid transport offers considerable promise for accelerating the rate of chemical and biochemical reactions through enhanced micromixing, and should thus benefit a wide range of practical applications.

RESULTS AND DISCUSSION

The enhanced fluid motion in the presence of tubular microengines is characterized by analysis of the mean squared displacement (MSD) of passive microsphere tracers. These MSD data illustrate that the transport in a suspension of bubble-propelled micromotors is substantially over the transport induced by suspensions of catalytic nanowires and Pt-Janus particle motors. Additional experiments in which the

Received: March 4, 2014
Revised: April 14, 2014
Published: April 23, 2014

   dx.doi.org/10.1021/la500819r | Langmuir 2014, 30, 5082−5087

tubular microengines were fixed to the glass slide were also used to separate the effect of the motor movement from that of the bubble generation, and to illustrate that the bubble evolution has a profound effect upon the observed enhanced transport of passive bead tracers.

The polymer-based microtubular engines were prepared by a template-based electrodeposition of poly(3,4-ethylenedioxythiophene) (EDOT) and COOH-EDOT/Pt bilayer[14] (see Experimental section in the Supporting Information (SI)). The template fabrication process resulted in ~8 μm-long polymer/Pt microtubes that propelled efficiently via the ejection of oxygen bubbles generated by the catalytic decomposition of hydrogen peroxide fuel at their inner Pt layer.[14] As will be discussed below, both the movements of the motors and of the bubbles they generate contribute to the marked increase in the effective diffusion coefficient of the 2 μm passive polystyrene-bead tracers. To examine the effect of motor movement and bubble generation on the transport of the passive tracers, equal volumes of four different solutions (of particles, micromotors, surfactant and fuel) were placed on a glass slide. The effect of ambient air motion and droplet spreading on particle transport was determined to be negligible by conducting a parallel experiment in the reservoir of a tailor-made PDMS chip, as will be described below. The movement of the micromotors and of their corresponding oxygen bubbles generated flow fields that caused the displacement of the passive tracers (Figure 1). The

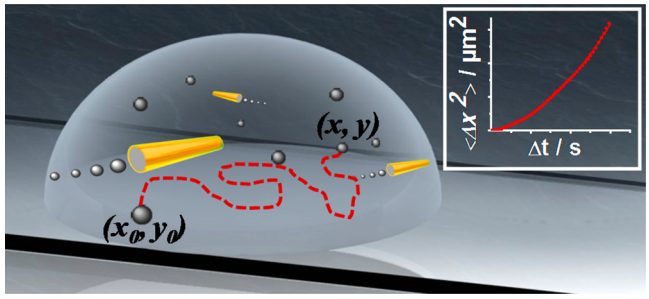

Figure 1. Schematic illustration of micromotor-enhanced transport of passive microparticle-tracers. Equal volume of solutions containing particles, micromotors, surfactant, and fuel were placed on a glass slide, and oxygen bubbles ejected from the self-propelled micromotors along with their own motion made the passive tracers displace from an initial to a final position denoted in the figure as (x_0, y_0) and (x, y), respectively. The enhanced motion rate of the particles is estimated by measuring their mean-square displacement $\langle \Delta x^2 \rangle$ at both short and long time intervals and its trend is studied upon such intervals, as shown in the inset at the top right of the figure.

motion of the particle tracers was video-recorded and analyzed with an automated particle-tracking software (see Experimental section for details). To minimize the influence of the three-dimensional fluid flow caused by the bubble collapse occurring at the top of the droplet, the passive bead tracers were only tracked near the bottom surface, where their motions and MSD were analyzed in two dimensions.

Figure 2 and SI Video 1 demonstrate the significantly enhanced diffusion of 2 μm passive polystyrene spherical particles due to the movement of bubble-propelled micro-tubular engines, compared to particles undergoing Brownian motion only. For example, Figure 2A,B display traces of the particle trajectories (during a 30 s period) and a plot of the mean squared displacement versus time, respectively, in the absence (a) and presence (b) of the hydrogen-peroxide fuel. In

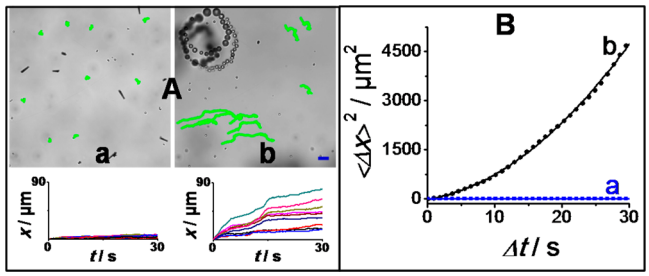

Figure 2. (A) Time-lapse images illustrating typical trajectories of nine particle tracers undergoing Brownian motion and a mixture of Brownian motion and convection using microtube engines in the absence and presence of the peroxide fuel, respectively. Typical tracking plots of the total distance traveled by the particles during 30 s are displayed at the bottom part of A (a and b), respectively. (B) Mean-squared displacement obtained by averaging over 100 particles, whose trajectories are subject to the effect of active micromotors swimming for 30s (b), with respect to that governed only by Brownian motion (a) upon time, at time intervals of 0.06 s. Enhanced transport of the passive tracers (2 μm, ~1.4×10^7/mL) is caused by the catalytic micromotors (8 μm, 4×10^6/mL) when self-propelled in aqueous solutions containing 5% Triton X-100 and 1.5% H_2O_2. Scale bar, 10 μm.

the absence of fuel (H_2O_2), both the micromotors and the tracer particles experience Brownian motion and thus the particle trajectories are chaotic and random, with negligible displacements (Figure 2a). In contrast, the bubble-propelled micromotors move rapidly in the presence of H_2O_2, leading to significantly enhanced fluid transport and displacement of the tracer particles (Figure 2b). The time-lapse images (A, top) illustrate the ability to simultaneously visualize and track both the tracer beads and the micromotors (with their microbubble tails). These images, and the corresponding tracking plots (shown at the bottom of A) indicate that the bead displacement is not uniform. As expected, the enhanced diffusion of the passive beads is strongly influenced by their position relative to the moving micromotors, being larger as the distance between the beads and the micromotors decreases. Unlike other catalytic motors, the tubular microengines tend to be inhomogeneously distributed in space (e.g., SI Video 2). Yet, as will be illustrated below, the average distance traveled by a large population of tracer particles(n = 100) is substantially greater than that observed in the presence of other common micromotors. The trajectories traced by the particles suggest that the nature of the flows they experience is coherent. This behavior is consistent with the hypothesis (discussed below) that the enhanced transport is greatly affected by the flow fields induced by the generated bubbles. The latter translate vertically and their flow fields are therefore relatively coherent compared to the flow fields induced by the translating micromotors, which follow random trajectories in arbitrary directions.

The transport is quantified in terms of the mean squared displacement (MSD) $\langle \Delta x^2 \rangle$ after a fixed time interval Δt, defined as

$$\left\langle \Delta x^2 \right\rangle|_{\Delta t} = \left\langle (x(\Delta t) - x_0)^2 + (y(\Delta t) - y_0)^2 \right\rangle \quad (1)$$

where the angle brackets $\langle \cdot \rangle$ indicate an average over an ensemble of n = 100 particles, subscript "0" denotes the original position of the tracer, and $x(\Delta t)$ and $y(\Delta t)$ are the coordinates of the particle in the plane of motion after time interval Δt. In general, the magnitude of the MSD reflects the strength of the

dx.doi.org/10.1021/la500819r | Langmuir 2014, 30, 5082−5087

transport, while its functional dependence on Δt characterizes the nature of this transport. In the case of pure Brownian motion in two dimensions, the MSD of a collection of spherical particles obeys:[31]

$$\langle \Delta x^2 \rangle = 4D\Delta t \quad (2)$$

Where D is the Brownian diffusivity of the particles. By analogy, a complex transport process involving a combination of diffusion and convection and such that the MSD grows linearly with time: $\langle \Delta x^2 \rangle \sim \Delta t$ (either within some interval Δt or for all times) is characterized as *diffusive*, and eq 2 can then be used to define an effective diffusion coefficient D. On the other hand, a purely *ballistic* motion of the particles results in the quadratic growth of the MSD with time: $\langle \Delta x^2 \rangle \sim \Delta t^2$, and more generally the transport is said to be *superdiffusive* if the MSD increases as $\langle \Delta x^2 \rangle \sim \Delta t^{\alpha}$, with $\alpha > 1$.[31] Over the time interval studied here, the enhanced diffusion of tracer particles due to bubble-propelled micromotors (in the presence of 1.5% H_2O_2) appears to be anomalous, with the MSD of the particles increasing nonlinearly with time as $\langle \Delta x^2 \rangle \sim t^{\alpha}$, with α >1.5 indicating superdiffusive transport. A superdiffusive behavior has been previously reported for the transport of passive tracer beads in a bath of motile bacteria.[31] In contrast, without the H_2O_2 fuel, tracer particles travel only by Brownian motion, and the data (shown in SI Figure 1) is consistent with normal diffusion with the MSD of the particles increasing linearly as a function of time (α = 1.0).

Figure 2B displays plots of $\langle \Delta x^2 \rangle$ versus time for the bead tracers in the absence (a) and presence (b) of the H_2O_2 fuel (and using the 5% Triton X-100 surfactant essential for the bubble evolution). The influence of micromotor activity (in the presence of the fuel) is clearly indicated from the dramatically larger MSD of the tracers as compared with pure Brownian motion, with D = 3.05 $\mu m^2\ s^{-1}$ (estimated from the maximum slope of MSD versus time over the time interval considered here) (b). In contrast, in the absence of fuel (Brownian motion), but in the presence of surfactant we obtain D = 0.024 $\mu m^2\ s^{-1}$. This value of D is about 1 order of magnitude lower than the theoretically calculated value using the Stokes–Einstein relation, $D = kT/6\pi\eta a$ = 0.21 $\mu m^2\ s^{-1}$ (with k Boltzmann constant, T temperature, η fluid viscosity, and a particle diameter). In order to gain further insights into this phenomenon, we conducted similar experiments in the absence of both the fuel and surfactant. This experiment resulted in a MSD corresponding to D = 0.17 $\mu m^2\ s^{-1}$, which is consistent with pure Brownian motion (see also SI Figure 1), and is close to the theoretical value expected for the "hindered diffusion" of particles near a solid no-slip surface.[34] The decrease in D by an order of magnitude in the presence of surfactant can be attributed to the generation of depletion forces between the particles and the glass slide,[35] which hold the particles close to the glass surface and enhance the hindered diffusion effect. In order to investigate possible contributions of ambient air motion and droplet spreading on the magnitude of D, we also conducted a series of experiments with drops confined in the reservoir of a PDMS chip. This effect was found to be negligible, as indicated by the value of D = 0.032 $\mu m^2\ s^{-1}$ for a Brownian motion experiment (in the presence of surfactant), which is close to the value estimated for the unconfined drop (D = 0.024 $\mu m^2\ s^{-1}$).

The substantial fluid transport imparted by tubular microengines is obvious upon comparison to other common catalytic micromotors (which are well-known to produce significantly less and greatly smaller bubbles). We conducted a series of experiments critically comparing the tracer transport induced by the bubble-propelled tubular microengines with that observed in the presence of common self-propelled nanowires and Janus microparticles. Figure 3 compares the MSDs of the

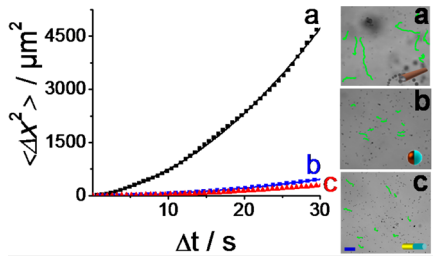

Figure 3. Effect of different types of micromotors on the enhanced transport of passive tracer particles. (Left) Plots comparing the average displacement of tracer particles by bubble-propelled PEDOT/Pt micromotors (a), Pt-SiO_2 Janus particles (b) and Au–Pt nanowires (c), swimming in an aqueous solution containing 1.5% H_2O_2 for 30 s. (Right) corresponding time-lapse images used for tracking of the motors (not to scale). Scale bar, 10 μm. Other conditions, as in Figure 2 (except that no Triton X-100 was used in b and c).

tracer particles over a 30 s period in suspensions of the different catalytic micromotors, including tubular microengines (a), Janus microparticles (b), and bimetallic nanowires (c), all powered by 1.5% H_2O_2 fuel (see also SI Videos 1 and 3). The calculated MSDs clearly indicate that the bubble-propelled microtubes induce a substantially greater tracer transport at all time intervals compared to the self-propelled Janus particles and bimetallic nanowires under the same fuel concentration (a vs b and c). For example, the MSD in the presence of bubble-propelled tubular microengines after 30 s (4679 μm^2) is around 10-fold and 16-fold larger compared to those induced by Pt-based Janus microparticles (442 μm^2) and Au–Pt nanowires (290 μm^2), respectively. The corresponding time-lapse images and particle trajectories in the presence of the different catalytic motors (shown on the right) clearly illustrate the significantly larger displacement of the tracer particles in the presence of tubular microengines (a), compared to nanowire (b) or Janus particle (c) motors. Even with a 3-fold increase of the fuel level of the nanowire and Janus-particle motors (to 5%), the bubble-propelled microengines (at 1.5% fuel) still led to a substantially enhanced fluid transport of the tracer particles (see SI Figure 2), with the MSD ca. 3-fold and 5-fold larger compared to those observed using Janus particles and nanowires, respectively. These data clearly demonstrate the advantage of the tubular microengines (over other catalytic micromotors) toward enhanced fluid transport and solution mixing.

A clear distinction between the self-propulsion of the different catalytic micromotors is the effective production of bubbles by the tubular microengines. In order to gain better understanding of the enhanced particle transport process associated with these microengines, we conducted a series of experiments aimed at distinguishing the relative contributions of the motor self-propulsion and of the bubble generation and motion on the enhanced transport of the tracer particles. For this purpose, we compared the fluid transport associated with freely moving microtube engines to the transport induced by bubbles generated by motors confined to the surface of the glass slide, coated with polymerized polylysine (see Supporting Information for details of the surface confinement and SI Video

dx.doi.org/10.1021/la500819r | Langmuir 2014, 30, 5082–5087

2 for bubble ejection). Figure 4 illustrates that at short times, the freely swimming micromotors induce the most vigorous

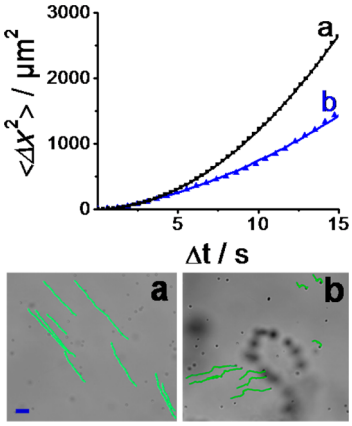

Figure 4. Effect of the bubbles (alone, without motion) on the enhanced transport of passive tracer particles. (Top) Average displacement of tracer particles by bubbles generated by stationary micromotors, confined to the surface of a glass slide (a), compared to that observed in the presence of freely swimming micromotors (b), at 1.5% H_2O_2/ 5% Triton-X 100 for 15 s. Other conditions as in Figure 2. (Bottom) corresponding time-lapse images; scale bar, 10 μm.

transport, but after ~3 s, the MSD for the bubbling-generating fixed motors surpasses that of the freely swimming motors. Note that the enhancement of fluid transport by the bubble-generating fixed motors is even greater than that of the freely swimming motors, because the latter tend to disperse and spread in space by self-propulsion, whereas fixed motors generate long-lived coherent flows near their point of anchor, thus dramatically enhancing tracer transport in their vicinity. We also found that when tracer particles are solely transported by the effect of bubbles, the MSD $\langle \Delta x^2 \rangle$ grows as Δt^2, indicating that the transport is ballistic and dominated by convection. The transport induced by the vertically rising bubbles dominates over the transport induced by the freely swimming motors, which is consistent with the nature of the flow fields generated in each case in the low-Reynolds-number regime. Indeed, the flow field generated by a rising bubble, which is acted upon by buoyancy forces and therefore exerts a net force on the fluid, decays slowly as $1/r$, where r is the distance to the center of the bubble. The moving micromotors, on the other hand, do not exert a net force on the fluid and produce a significantly weaker flow field that decays more rapidly as $1/r^2$. Such dependences could be used to develop theoretical estimates for the observed differences in tracer transport, although deriving such would require knowledge of the statistics of the motor and particle distributions in the fluid and are beyond the scope of this study. Further evidence of the importance of bubbling can be seen in the particle trajectories plotted in Figure 4A,B, where the direction of the particle trajectories appears constant over 15s. This is consistent with the view that the particles are primarily transported by the flow field generated by the vertically translating bubbles (as opposed to the self-propelled micromotors which move in many arbitrary directions).

Figure 5 demonstrates the increase in the tracer particle transport with increased micromotor activity associated with higher fuel concentrations. Increasing the H_2O_2 concentration from 1.0 to 1.5% (b–d), leads to increased bubble frequency

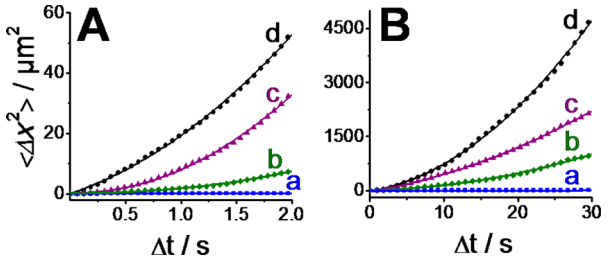

Figure 5. Enhanced transport of passive tracers upon increasing concentrations of H_2O_2. Average mean-squared displacements of 100 tracer particles at short (a) and long (b) time intervals, with 0 (a), 1.0 (b), 1.25 (c) and 1.5% (d) H_2O_2 fuel concentration, respectively. Other conditions as in Figure 2.

and motor self-propulsion, thus resulting in an increased tracer transport. Interestingly, the trend in the plot of $\langle \Delta x^2 \rangle$ versus Δt for different H_2O_2 concentrations is similar for both the short and long time intervals examined (A vs B for 2 s and 30 s, respectively), with the MSD increasing from 1010 to 4694 μm^2 for 1.0 and 1.5% peroxide levels, respectively, after a 30 s interval. Overall, the data of Figure 5 indicates a large increase in the tracer MSD with increasing fuel concentrations for long time intervals.

Finally, we examined the influence of the density of the micromotors upon the fluid transport using a fixed (1.0%) H_2O_2 fuel concentration. The results, shown in SI Figure 3, illustrate a similar trend for the MSD versus Δt for motor densities of 4×10^6 versus 8×10^6/mL, i.e., a nonlinear (superdiffusive) time dependence. Also note that doubling the motor density leads to a ~2-fold increase in the MSD (2078.7 vs 989.3 μm^2) after long times (30 s), suggesting a linear relationship between the motor density and the induced transport within the regime studied here.

CONCLUSION

We have reported a fundamental study of the effect of bubble-propelled tubular microengines on the enhanced diffusion of passive microsphere tracers. These active microtubular motors were found to substantially increase the displacement of tracer microparticles through fluid convection from the bubbles produced during their self-propulsion. The study sheds useful insights toward understanding the influence of the motion of multiple micromotors, bubble generation, and additional factors (*e.g.*, motor density, fuel concentration) upon the enhanced transport. In particular, the study highlights the unique role played by the bubble generation upon such dramatically enhanced transport. Because of the strong coherent flows driven by the rising bubbles emitted by the motors, the enhanced passive tracer transport and fluid motions observed in the presence of tubular microengines were found to be substantially larger than for other common catalytic micromotors, including bimetallic nanowires and Pt-Janus microparticles. These findings have important implications upon the use of tubular microengines and microbubbles for mixing reagents and accelerating the rate of chemical and biochemical reactions (compared to quiescent conditions). Such motor-induced fluid mixing capability thus holds considerable promise for enhancing the yield and speed of a wide range of chemical processes. It holds particular promise in situations where external mechanical stirring is not possible or not desired (e.g., using microscale volumes, lab-on-a-chip formats, or in hostile remote settings).

dx.doi.org/10.1021/la500819r | *Langmuir* 2014, 30, 5082–5087

■ ASSOCIATED CONTENT

Supporting Information

Experimental section, additional figures and videos. This material is available free of charge via the Internet at http://pubs.acs.org.

■ AUTHOR INFORMATION

Corresponding Authors

*E-mail: dsaintillan@eng.ucsd.edu.
*E-mail: josephwang@ucsd.edu.

Author Contributions

The manuscript was written through contributions of all authors. All authors have given approval to the final version of the manuscript.

Notes

The authors declare no competing financial interest.

■ ACKNOWLEDGMENTS

This project received support from the Defense Threat Reduction Agency-Joint Science and Technology Office for Chemical and Biological Defense (Grant no. HDTRA1-13-1-0002). B.J.-S. acknowledges support from the People Programme (Marie Curie Actions) of the EU 7th Framework Programme (FP7 2007-2013) under REA Grant PIOF-GA-2012-326476. D.S. acknowledges support from NSF CAREER Grant CBET-1150590. W.G. is a HHMI International Student Research fellow.

■ REFERENCES

(1) Wang, J. *Nanomachines: Fundamentals and Applications*; Wiley-VCH: Weinheim, Germany, 2013.
(2) Wang, W.; Duan, W.; Ahmed, S.; Mallouk, T. E.; Sen, A. Small power: Autonomous nano- and micromotors propelled by self-generated gradients. *Nano Today* **2013**, *8*, 531−554.
(3) Mirkovic, T.; Zacharia, N. S.; Scholes, G. D.; Ozin, G. A. Fuel for thought: Chemically powered nanomotors out-swim nature's flagellated bacteria. *ACS Nano* **2010**, *4*, 1782−1789.
(4) Mei, Y.; Solovev, A. A.; Sanchez, S.; Schmidt, O. G. Rolled-up nanotech on polymers: From basic perception to self-propelled catalytic microengines. *Chem. Soc. Rev.* **2011**, *40*, 2109−2119.
(5) Sanchez, S.; Pumera, M. Nanorobots: The ultimate wireless self-propelled sensing and actuating devices. *Chem.—Asian J.* **2009**, *4*, 1402−1410.
(6) Wilson, D. A.; Nolte, R. J. M.; van Hest, J. C. M. Autonomous movement of platinum-loaded stomatocytes. *Nat. Chem.* **2012**, *4*, 268−274.
(7) Pumera, M. Electrochemically powered self-propelled electrophoretic nanosubmarines. *Nanoscale* **2010**, *2*, 1643−1649.
(8) He, Y.; Wu, J.; Zhao, Y. P. Designing catalytic nanomotors by dynamic shadowing growth. *Nano Lett.* **2007**, *7*, 1369−1375.
(9) Wang, W.; Chiang, T.; Velegol, D.; Mallouk, T. E. Understanding the efficiency of autonomous nano- and microscale motors. *J. Am. Chem. Soc.* **2013**, *135*, 10557.
(10) Paxton, W. F.; Kistler, K. C.; Olmeda, C. C.; Sen, A.; St. Angelo, S. K.; Cao, Y.; Mallouk, T. E.; Lammert, P. E.; Crespi, V. H. Catalytic nanomotors: Autonomous movement of striped nanorods. *J. Am. Chem. Soc.* **2004**, *126*, 13424−13431.
(11) Fournier-Bidoz, S.; Arsenault, A. C.; Manners, I.; Ozin, G. A. Synthetic self-propelled nanomotors. *Chem. Commun.* **2005**, 441−443.
(12) Mei, Y. F.; Huang, G. S.; Solovev, A. A.; Urena, E. B.; Monch, I.; Ding, F.; Reindl, T.; Fu, R. K. Y.; Chu, P. K.; Schmidt, O. G. Versatile approach for integrative and functionalized tubes by strain engineering of nanomembranes on polymers. *Adv. Mater.* **2008**, *20*, 4085−4090.
(13) Solovev, A. A.; Mei, Y. F.; Urena, E. B.; Huang, G. S.; Schmidt, O. G. Catalytic microtubular jet engines self-propelled by accumulated gas bubbles. *Small* **2009**, *5*, 1688−1692.
(14) Gao, W.; Sattayasamitsathit, S.; Orozco, J.; Wang, J. Highly efficient catalytic microengines: Template electrosynthesis of polyaniline/platinum microtubes. *J. Am. Chem. Soc.* **2011**, *133*, 11862−11864.
(15) Zhao, G.; Pumera, M. Concentric bimetallic microjets by electrodeposition. *RSC Adv.* **2013**, *3*, 3963−3966.
(16) Howse, J. R.; Jones, R. A.; Ryan, A. J.; Gough, T.; Vafabakhsh, R.; Golestanian, R. Self-motile colloidal particles: From directed propulsion to random walk. *Phys. Rev. Lett.* **2007**, *99*, 048102.
(17) Gibbs, J. G.; Zhao, Y.-P. Autonomously motile catalytic nanomotors by bubble propulsion. *Appl. Phys. Lett.* **2009**, *94*, 163104.
(18) Baraban, L.; Makarov, D.; Streubel, R.; Monch, I.; Grimm, D.; Sanchez, S.; Schmidt, O. G. Catalytic Janus motors on microfluidic chip: Deterministic motion for targeted cargo delivery. *ACS Nano* **2012**, *6*, 3383−3889.
(19) Gao, W.; Pei, A.; Feng, X.; Hennessy, C.; Wang, J. Organized self-assembly of Janus micromotors with hydrophobic hemispheres. *J. Am. Chem. Soc.* **2013**, *135*, 998−1001.
(20) Solovev, A. A.; Sanchez, S.; Pumera, M.; Mei, Y. F.; Schmidt, O. G. Magnetic control of tubular catalytic microbots for the transport, assembly, and delivery of micro-objects. *Adv. Funct. Mater.* **2010**, *20*, 2430−2435.
(21) Zhao, G.; Wang, H.; Sanchez, S.; Schmidt, O. G.; Pumera, M. Artificial micro-cinderella based on self-propelled micromagnets for the active separation of paramagnetic particles. *Chem. Commun.* **2013**, *49*, 5147−5149.
(22) Abdelmohsen, L. K. E. A.; Peng, F.; Tu, Y.; Wilson, D. A. Micro- and nano-motors for biomedical applications. *J. Mater. Chem. B* **2014**, *2*, 2395−2408.
(23) Wang, J.; Gao, W. Nano/microscale motors: Biomedical opportunities and challenges. *ACS Nano* **2012**, *6*, 5745−5751.
(24) Campuzano, S.; Orozco, J.; Kagan, D.; Guix, M.; Gao, W.; Sattayasamitsathit, S.; Claussen, J. C.; Merkoci, A.; Wang, J. Bacterial isolation by lectin-modified microengines. *Nano Lett.* **2012**, *12*, 396−401.
(25) Solovev, A. A.; Xi, W.; Gracias, D. H.; Harazim, S. M.; Deneke, C.; Sanchez, S.; Schmidt, O. G. Self-propelled nanotools. *ACS Nano* **2012**, *6*, 1751−1756.
(26) Orozco, J.; García-Gradilla, V.; D'Agostino, M.; Gao, W.; Cortés, A.; Wang, J. Artificial enzyme-powered microfish for water-quality testing. *ACS Nano* **2013**, *7*, 818−824.
(27) Orozco, J.; Cheng, G.; Vilela, D.; Sattayasamitsathit, S.; Vazquez-Duhalt, R.; Valdes-Ramirez, G.; Pak, O. S.; Escarpa, A.; Kan, C.; Wang, J. Micromotor-based high-yielding fast oxidative detoxification of chemical threats. *Angew. Chem., Int. Ed.* **2013**, *52*, 13276−13279.
(28) Soler, L.; Magdanz, V.; Fomin, V. M.; Sanchez, S.; Schmidt, O. G. Self-propelled micromotors for cleaning polluted water. *ACS Nano* **2013**, *7*, 9611−9620.
(29) Kim, M. J.; Breuer, K. S. Enhanced diffusion due to motile bacteria. *Phys. Fluids* **2004**, *9*, L78−L81.
(30) Sokolov, A.; Goldstein, R. E.; Feldchtein, F. I.; Aranson, I. S. Enhanced mixing and spatial instability in concentrated bacterial suspensions. *Phys. Rev. E* **2009**, *80*, 031903.
(31) Wu, X. L.; Libchaber, A. Particle diffusion in a quasi-two-dimensional bacterial bath. *Phys. Rev. Lett.* **2000**, *13*, 3017−3020.
(32) Miño, G.; Mallouk, T. E.; Darnige, T.; Hoyos, M.; Dauchet, J.; Dunstan, J.; Soto, R.; Wang, Y.; Rousselet, A.; Clement, E. Enhanced diffusion due to active swimmers at a solid surface. *Phys. Rev. Lett.* **2011**, *106*, 048102.
(33) Dunderdale, G.; Ebbens, S.; Fairclough, P.; Howse, J. Importance of particle tracking and calculating the mean-squared displacement in distinguishing nanopropulsion from other processes. *Langmuir* **2012**, *28*, 10997−11006.
(34) Huang, P.; Breuer, K. S. Direct measurement of anisotropic near-wall hindered diffusion using total internal reflection velocimetry. *Phys. Rev. E* **2007**, *76*, 046307.

(35) Asakura, S.; Oosawa, F. Interaction between particles suspended in solutions of macromolecules. *J. Polym. Sci.* **1958**, *33*, 183−192.

dx.doi.org/10.1021/la500819r | *Langmuir* 2014, 30, 5082−5087